RSC Advances

ROYAL SOCIETY OF CHEMISTRY

www.rsc.org/advances

Spongy Nitrogen-Doped Activated Carbonaceous Hybrid Derived from Biomass Material/Graphene Oxide for Supercapacitor Electrodes

Samira Gharehkhani,[*, †] *Seyed Farid Seyed Shirazi,* [*, ‡] *Siamak Pilban Jahromi,* [§] *Mehran Sookhakian,* [§] *Saeid Baradaran,* [†] *Hooman Yarmand,* [†] *Azim Ataollahi Oshkour,* [†] *Salim Newaz Kazi,* [†] *Wan Jefrey Basirun* [‖, #]

[†] Department of Mechanical Engineering, Faculty of Engineering, University of Malaya, 50603 Kuala Lumpur, Malaysia.

[‡] Department of Mechanical Engineering and Advanced Material Research Center, University of Malaya, 50603, Kuala Lumpur, Malaysia.

[§] Low Dimensional Materials Research Center, Department of Physics, Faculty of Science, University of Malaya, 50603, Kuala Lumpur, Malaysia.

[‖] Institute of Nanotechnology & Catalysis Research (NanoCat), University of Malaya, 50603 Kuala Lumpur, Malaysia.

[#] Department of Chemistry, Faculty of Science, University of Malaya, 50603, Kuala Lumpur, Malaysia.

ABSTRACT

Carbon derived from low cost agricultural waste material was used as a precursor for the preparation of spongy-like nitrogen doped activated composite from carbon/graphene oxide via a one-step thermal treatment. N-doping and activation of the carbon/graphene oxide mixture were achieved simultaneously by the treatment of urea and potassium hydroxide at 800 ºC. The nitrogen content and ratio between the nitrogen species was controlled by the mass ratio of KOH:carbon. The composite was prepared with a KOH:carbon ratio of 1 which resulted in a moderate surface area (1712.4 m^2 g^{-1}) and a high nitrogen content (14.51 %). The hybrid material gave high specific capacitance (267 F g^{-1} at 5 mV s^{-1}) and good cycling stability (92.3% capacitance retention after 5000 cycles) in 6 M KOH electrolyte. Hence, the new composite presented in this work can be used as an advanced material for supercapacitor applications.

Keywords: Biomass Carbon; Graphene oxide; Nitrogen Doped; Supercapacitor

1. INTRODUCTION

Energy storage devices are attracting intense research due to the high rate of production of electronic systems, and increasing concerns of global warming and non-renewable fossil fuels. One of the best candidates for the energy storage devices is electrochemical capacitors, which have high specific capacitance, low maintenance cost and excellent cycling stability.

Based on the reaction mechanism, electrochemical capacitors are categorized into electrical double layer capacitors (EDLCs) and pseudocapacitors[1-3]. The materials which are used as EDLCs have acceptable electrical conductivity and good cycle life, but they often suffer from the low specific capacitance. Unlike the first category of electrochemical capacitors (EDLCs), pseudocapacitors have good specific capacitance due to the Faradaic reactions, although the lower electrical conductivity and cycling stability would limit their applications[4]. With regards to the advantages and disadvantages of both categories of electrochemical capacitors, it can be concluded that the introduction of materials with higher specific capacitance, cycle life and electrical conductivity could lead to wider applications of such materials.

Among the different types of electrode materials, such as conductive polymers[5], graphene [6] and carbon nanotubes[7-9], the carbons with high surface area (activated carbon (AC)) have been used commercially for EDLC applications[10, 11]. Fossil-fuel based precursors, and biomass materials can be used to prepare the AC[12-16]. Compared to the fossil-fuel materials, these biomass precursors are cheaper and environmental friendly. Oil palm empty fruit bunch (EFB), a non-wood fiber [17] is a suitable biomass precursor for the preparation of AC. EFB is the primary solid waste of palm oil mill processing and is abundant in south east Asia. The annual production of crop residue in the oil palm mills is estimated around 33 million tons in the form of EFB, fiber and shell. Hence, the lignocellulosic EFB is a low-cost and commercially available material for the production of carbonaceous substances [18].

AC can be produced by either physical or chemical activation process. In the physical activation process, an activation gas e.g., CO_2, steam or mixture of gases is used to prepare the activated carbon. In the chemical activation process, the carbon precursor are mixed with chemical reagents such as $ZnCl_2$, H_3PO_4, NaOH and KOH [19]. The use of KOH in the activation process was reported previously[14, 15, 20]. Compared to other reagents such as $ZnCl_2$, KOH is more eco-friendly, therefore is more preferred in the chemical activation process [21].

Capacity improvement of porous carbons is one of the main focus areas in electrochemical studies[22]. Recently, different approaches such as the synthesis of a high surface area carbon using a composite containing carbon and graphene, has been reported[23, 24]. Graphene, a 2D single layer of sp^2 carbon atoms, exhibits very high electrical conductivity [25]. Many studies have been reported on the electrochemical properties and capacitor performances of different types of graphene with a variety of chemical and morphological structures such as graphene oxide (GO), graphene nanoplatelet and reduced graphene oxide (RGO)[26-30]. The different methods for the reduction of GO includes the use of chemicals such as hydrazine hydrate, or reduction via high temperature thermal treatment have been reported[6, 31, 32]. Although graphene based compounds are excellent materials for capacitor applications, the synthesis of graphene in large batch is difficult and expensive. Moreover, the limited surface area of graphene despite its high theoretical surface area (2630 m^2 g^{-1}) is another disadvantage. By considering these facts, it could be conceived that the use of graphene as a guest material in an amorphous carbon could be more efficient and augments the electrical conductivity and charge-carrier mobility of the composite.

Another alternative strategy is to improve the capacitance of the carbon materials by doping the carbon networks with heteroatoms such as nitrogen and oxygen, which can improve the charge transfer along the carbon network[33-35]. Moreover, the surface groups on the carbon materials may induce an acid-base property, which could improve the capacitance of the

carbon materials through the pseudocapacitance reactions[36, 37]. The incorporation of nitrogen atoms into a carbon network has been accomplished by treatment methods using ammonia or urea[38], or *in situ* doping methods using nitrogen source precursors such as melamine resin[39], polyvinylpyridine[40], polypyrrole[41], polyaniline[42] and chitosan[43]. Zhao, et al. [44] synthesized porous nitrogen doped composite via co-pyrolysis of lignosulfonate and GO. Urea was used as the nitrogen source and the nanoporous structure with a nitrogen content of 7.41 % gave high capacitance value with 92.5% capacitance retention after 1000 cycles.

It is more worthwhile to synthesize materials with high capacitance from renewable sources, with a facile single-step and scalable synthetic process. Therefore, in this report, for the first time, we introduce a spongy-like structured composite containing a carbon derived from agricultural waste materials and GO which was synthesized via the simultaneous nitrogen doping and activation process for supercapacitor electrodes. This green, low cost, facile and effective single-step approach was employed to prepare a nitrogen doped activated carbon/RGO composite which has bright prospect as an extraordinary material for electrochemical applications.

2. EXPERIMENTAL SECTION

2.1. Materials synthesis

2.1.1. Preparation of the carbon sample

EFB fiber was pyrolysed at 500 ºC with a heating rate of 10 ^{o}C min^{-1} for 2 hours in a N_2 saturated atmosphere. The prepared carbon was ground into fine powders by ball milling for 5 min. This was followed by the addition of the grounded carbon (1 g) in 100 ml KOH/Urea (1 g/5 g) aqueous solution with continuous stirring at 500 rpm for 2 hours. Another sample also was prepared by the addition of 1 g of carbon in 100 ml KOH/Urea (4 g/5 g) aqueous solution.

2.1.2. Preparation of GO sample

The GO was prepared using the Hummer's method. The GO (3 wt% of carbon) was dispersed in deionized water (50 ml) by sonication for 30 min. Then the GO solution was mixed with 100 ml aqueous mixture of KOH and urea at two different mass ratios of 1:1:5 and 1:4:5, followed by stirring at 500 rpm for 2 hours.

2.1.3. Preparation of N-doped activated composite

In this step, the carbon and GO samples were mixed and stirred for 3 hours. The solution was dried at 50 ºC. The dried mixture was then placed in an alumina crucible in a tube furnace. The mixture was heated at a rate of 5 ºC min^{-1} under N_2 flow at 430 ºC for 30 minutes, and heated to 800 ºC for 75 minutes. The obtained sample was thoroughly washed with 0.1 M HCl and deionized water to remove the impurities and to obtain a neutral pH. Finally, the samples were dried at 60 ^{o}C and denoted as NA-CRGO-1 and NA-CRGO-4 according to the KOH:C weight ratio.

To study the effect of GO and nitrogen doping on the sample properties, three series of undoped samples with and without GO and impregnated only with the KOH (denoted as AC, A-CRGO-1 and A-CRGO-4) were prepared as the control samples. The AC sample was prepared with a KOH: C ratio of 4. Moreover GO was thermally reduced to RGO during the process, hence a thermally reduced graphene oxide (RGO) sample was prepared from the heating of GO (without agents) in the furnace, with the same procedure.

2.2. Characterization

The pore structure of the samples was analyzed with a surface area and porosity analyzer (BELSORP-max nitrogen adsorption apparatus (Japan, Inc.). The microscopic morphology of the prepared samples was observed using a high-resolution FEI Quanta 200F field emission

scanning electron microscope (FESEM) and a transmission electron microscope (TEM, Zeiss Libra 120). The samples were prepared for TEM characterization by dispersing the powder in ethanol, placing it onto the micro grid, and evaporating the solvent. Raman characterization was obtained using a Renishaw Invia Raman Microscope with laser excitation at 514 nm. X-ray photoelectron spectroscopy (XPS) measurements were performed using a monochoromated Al Kα excitation source.

2.3. Electrochemical measurements

A three-electrode electrochemical cell with graphite as the counter-electrode and Hg/HgO as the reference in 6M KOH aqueous solution were used in the electrochemical experiments. The working electrodes were prepared by mixing the as-prepared materials with Polyvinylidene fluoride (PVDF) (solution in N-methyl 2-pyrrolidone) at a ratio of 90:10, by weight. Then the mixtures were coated onto a 1 cm^2 nickel foil, and dried at 70 ºC for 12 hours. The total mass of the coated material on the foil was between 3-4 mg. Cyclic voltammogram (CV) and galvanostatic charge/discharge curves were obtained using an electrochemical workstation (Potentiostat/Galvanostat Model PGSTAT-302 N from Autolab, controlled by a USB_IF030 interface card and GPES software installed on a computer). The electrochemical impedance spectroscopy (EIS) measurements were also carried out by an AC voltage with 10 mV amplitude with a frequency range from 0.01 Hz to 100 KHz at the open circuit potential.

The specific capacitance of the electrodes were calculated from the CV curves using Equation 1 where C_s is the specific capacitance of the sample (F g^{-1}), v is the scan rate (V s^{-1}), m is the mass of active material (g), ΔV_{if} is the applied potential window, and the integral term is equal to the area under the CV curve.

$$C_s = \frac{1}{vm.\Delta V_{if}} \int_{V_i}^{V_f} I \times V dV \quad (1)$$

3. RESULTS AND DISCUSSION

3.1 Structural properties

Figure 1 (a-f) shows the FESEM images of pure AC and NA-CRGO samples. These images present the attachment of RGO to carbon which forms a spongy crumpled structure. The EFB derived-carbon containing the fiber bundles and RGO can be clearly observed in the FESEM images. Further morphology studies have been conducted by TEM. TEM images of pure AC, RGO, NA-CRGO-1, NA-CRGO-4, A-CRGO-1 and A-CRGO-4 are presented in Figure 2 (a-d) and S1 (Supporting Information). The TEM images also confirm the contribution of RGO in the matrix structure.

The activation process with higher amount of KOH leads to a larger exposition of the amorphous structure of carbon, which is due to the amount of gases produced during the activation process by KOH. Figure 2c and 2d show that the simultaneous N doping and activation process produced more wrinkles to the structure as compared to activation process (Figure S1 (a and b)). However an increase in mass ratio of KOH:carbon leads to a higher porosity and surface roughness. On the other hand, N doping introduces more wrinkles to the surface. The distribution of the nitrogen atoms in NA-CRGO-1 structure was further characterized by FESEM elemental mapping (Figure 2e). The homogeneous distribution of the nitrogen atoms shows that nitrogen can be properly doped in the composites. However, it seems that there is a slight difference between the amounts of N doped atoms into the composite components. The energy dispersive X-ray (EDX) data for NA-CRGO-1 (Figure S2) demonstrated that RGO (zone 1) in the composite probably has more affinity to accept foreign atoms than carbon (zone 2).

The nitrogen adsorption/desorption isotherm and pore size distributions of the N-doped samples, are presented in Figure 3a and 3b respectively. The isotherms in Figure 3a show type I curve, based on the International Union of Pure and Applied Chemistry (IUPAC), which presents a microporous structure with small amount of mesoporous appearance for the NA-CRGO-1 and NA-CRGO-4. Figure 3b presents the pore size distribution curves which show that the NA-CRGO-4 has higher pore volume than NA-CRGO-1 due to the ratio of the KOH:C. The pore size of the samples is basically less than 2 nm. Besides the micropores, the contribution of meso scale pores with size more than 2 nm, can be seen in the micro-graphs which could facilitate the transportation of the electrolyte ions[45, 46]. The estimated surface areas based on the Brunauer–Emmett–Teller (BET) method and pore structure characterization data for N-doped samples are presented in Table 1. The estimated BET specific surface areas are 1712.4 and 2261.2 $m^2 g^{-1}$ for NA-CRGO-1 and NA-CRGO-4, respectively, which demonstrates an ultrahigh surface area compared to the untreated carbon (7.5 m^2g^{-1}). The BET surface area of GO reported in the literatures is less than 100 m^2g^{-1} [47, 48]. Moreover, the micropore to mesopore volume ratio has decreased from 2.87 for NA-CRGO-1 to 1.83 for NA-CRGO-4, respectively.

Generally, the use of KOH for the preparation of activated carbon yields a carbon structure with high surface area, high microporous structure and a narrow pore size distribution. To describe the mechanism of activation with KOH, it was proposed that the alkali metal intercalates in the carbon lattice and acts as an electron donor which promotes the reaction during gasification [21, 49]. The reaction between KOH and carbon can be described in the following reaction:

$$6KOH + 2C \leftrightarrow 2K + 3H_2 + 2K_2CO_3$$ [50, 51] (2)

When the activation temperature is higher than 700 °C , the following reactions may occur [52]

$K_2CO_3 \rightarrow K_2O + CO_2$ (3)

$K_2CO_3 \rightarrow 2C + 2K_2O$ (4)

$K_2O + C \rightarrow 2K + CO$ (5)

Raman spectroscopy is a powerful tool for the investigation of structural changes of carbon materials. The peak intensity of the D and G bands in the Raman spectra are shown in Figure 3c. The Raman spectra of the prepared samples show the D-band at ~1340 cm^{-1} and the G-band at ~1598 cm^{-1}. Compared with A-CRGO-1 and A-CRGO-4, the G peak of NA-CRGO-1 and NA-CRGO-4 exhibit a slight blue shift. One of the most important parameters in the Raman spectrum is the peak intensity ratio of the D and G bands, (I_D/I_G) which is attributed to the disordered crystal structures of the carbon material. The I_D/I_G values for NA-CRGO-4, NA-CRGO-1, A-CRGO-4, A-CRGO-1 and AC, are 0.73, 0.61, 0.51, 0.42 and 0.36, respectively. It is noted that an increase in the I_D/I_G in the NA-CRGO samples prepared from the combination of N-doping and activation processes lead to a less degree of graphitization which probably resulted from the incorporation of N atoms[53]. Moreover, the Raman spectra of GO and RGO are presented in Figure S3. The I_D/I_G values of GO and RGO are 0.60 and 0.95, respectively. The increase of the I_D/I_G of RGO compared to GO confirms the reduction of GO to RGO [54, 55].

Table 2 presents the chemical composition of the samples, from the XPS data. Moreover the total carbon, hydrogen, oxygen and nitrogen contents (%) in AC, A-CRGO and NA-CRGO samples obtained by the elemental analysis (CHN) method was utilized in initial analysis of the samples (Table S1).

The difference between the CHN and XPS results is due to the fact that CHN determines the bulk composition of each elements, while XPS presents the surface composition of the elements[37]. In order to reveal the elemental composition of the surface clearly, the resulting XPS spectra are displayed in Figure 4. As shown in Figure 4a, the N 1s peak is only present

in the NA-CRGO samples, but not in the A-CRGO and AC samples. The N 1s peak in the nitrogen doped samples (NA-CRGO-1 and NA-CRGO-4) was deconvoluted into three different regions. The three nitrogen functional groups (Figure 4b and 4c) are pyridinic-N (N1, ~ 398 eV), pyrrolic-N (N2, ~ 400 eV) and quaternary-N (N3, ~ 401 eV). As listed in Table 2, the NA-CRGO-1 consists more nitrogen atoms as well as higher N:C ratio compared to NA-CRGO-4, which shows the possibility of the increase of N content by decreasing the KOH dosage[34, 56]. The dominant sites in both N doped samples are pyridinic nitrogen and pyrrolic nitrogen and NA-CRGO-1 shows a proper ratio of nitrogen species with more quaternary nitrogen atoms. Figure 4d and 4e present the C1s core level peak of the NA-CRGO-1 and NA-CRGO-4 respectively. The main peak at 284.5eV corresponds to C=C. The three small peaks located at 285.50, 287.08 and 288.38 eV; and 285.42, 286.68 and 287.98 eV in the NA-CRGO-1 and NA-CRGO-4 spectra respectively, are ascribed to C=N & C-O, C-N & C=O and O-C=O. Although the peaks at around 285 and 287 eV are usually assigned to the C-O and C=O respectively, this peak could be attributed to the C=N and C-N in the nitrogen doped samples[57]. In addition, Table 2 reveals a lower oxygen content in the NA-CRGO samples compared to the A-CRGO samples. The O 1s peaks of NA-CRGO-1 and NA-CRGO-4 (Figure S4) can be deconvoluted into the C=O, C-OH & C-O-C and COOH carboxylic groups and water[47]. A schematic structure of the nitrogen surface functional groups on carbon is shown in Figure 4f.

3.2. Electrochemical Properties

A three electrode system was used to evaluate the electrochemical properties of the present samples. From the sample characterization results, it is expected that the NA-CRGO samples exhibit higher electrochemical performance. A series of electrochemical tests have been conducted on the NA-CRGO samples to examine their capacitance properties and compared

to the undoped samples i.e. A-CRGO-1 and A-CRGO-4. Figure 5a shows the CV curves between -1 V to 0 V at 10 mV s^{-1}, which are oblique quasi-rectangular. As can be seen, the NA-CRGO-1 has a wider curve and higher current density compared to the other samples. The NA-CRGO samples show small redox peaks at around -0.6 V, while the A-CRGO samples reveal curves with no humps. The calculated specific capacitance for NA-CRGO-1 is 267 F g^{-1} in 6 M KOH at 5 mV s^{-1}, which is higher than NA-CRGO-4 (210 F g^{-1}), A-CRGO -1 (128 F g^{-1}), A-CRGO-4 (147 F g^{-1}), AC (121 F g^{-1}) and RGO (34 F g^{-1}) obtained under the same conditions. Results show that: 1) the specific capacitance of AC is lower compared to A-CRGO-4. A comparison of the capacitance of AC and A-CRGO-4 confirms the influence of graphene in the increase of the specific capacitance [23]. 2) The doped samples have higher capacitance which is attributed to the combination of EDLC, and redox reactions due to the presence of surface functional groups. The presence of nitrogen and oxygen functional groups on the surface is responsible for the pseudocapacitance behavior of the doped samples[27]. It can be claimed that the pseudocapacitance contribution is mostly due to the presence of the nitrogen functional groups and not to the oxygen groups in the NA-CRGO samples, as the A-CRGO samples (prepared by the same process as the NA-CRGO but without the nitrogen precursor) show no hump in the CV curves. This also coincides with the XPS results which show that the A-CRGO samples contain more oxygen groups compared to the NA-CRGO samples. Therefore, the absence of the redox peaks in the A-CRGO samples confirms the role of nitrogen atoms in the Faradaic reactions of the NA-CRGO samples. 3) Among the N-doped samples, the NA-CRGO-1 with lower surface area has higher capacitance than NA-CRGO-4 with higher surface area. The specific capacitance is not directly proportional to the specific surface area, is due to the decrease in the nitrogen content, from the higher amount of KOH which increases the surface area of the material. It has been reported that substantial detriment in the nitrogen functionalities is due to oxidation

[36, 58]. When the amount of doped nitrogen content in the material decreases, the pseudo-capacitance also decreases, and resulting in a decrease of the capacitance value. Another reason is that most of the surface area may not be accessible to the electrolyte ions [59]. The doping of nitrogen can increase the wetabillity via the increase of hydrophilic surface functional groups, hence the electrolyte can fill more pores. Therefore, the increase in the amount of N doped atoms can increase the electroactive surface area [52].

The CV profiles and the relation between the specific capacitance and scan rate for the NA-CRGO-1 and NA-CRGO-4 are shown in Figures 5b-d. The same trend can be observed in the NA-CRGO samples. The decrease of specific capacitance for NA-CRGO-1 at scan rate 5 mV s^{-1} to 20 mV s^{-1} is more profound compared to the scan rate from 20 mV s^{-1} to 100 mV s^{-1} which can be attributed to a higher contribution of the pseudocapacitance behavior in lower scan rates (Figure 5d).

The specific capacitance for NA-CRGO-1 is comparable with the reported N-doped porous carbons [44], which is probably due to the proper structure of the material which can increase the electrolyte penetration and facilitate the transport of electrons in the active material, and an appropriate ratio of edge nitrogen atoms (N1 and N2) to N3[60] .

Figure 6 (a) and (b) show the galvanostatic charge-discharge curves for all samples at 0.3 A g^{-1}, and NA-CRGO-1 at different current densities respectively. The specific capacitance calculated from the galvanostatic discharge curves at 0.3 A g^{-1} are 214, 175, 86, 99, 80 and 25 F g^{-1} for NA-CRGO-1, NA-CRGO-4, A-CRGO-1, A-CRGO-4, AC and RGO respectively.

The EIS test was performed to further investigate the electrochemical behavior of the N-doped samples. The Nyquist plots show a semicircle at higher frequency region and a straight line at lower frequency region for the samples (Figure 6c). The characteristic impedance plots for AC and RGO are also presented in Fig. 6c. The NA-CRGO-1 has a larger slope compared to NA-CRGO-4, which confirms its ideal capacitive behavior[27, 57]. Furthermore,

the diameter of the semicircle is an indication of the charge transfer resistance and electrode conductivity[61]. The NA-CRGO-1 shows a smaller semicircle diameter compared to NA-CRGO-4. It can be concluded that NA-CRGO-1 has lower charge transfer resistance, which is due to the higher amount of quaternary-N atoms. Moreover, the NA-CRGO-4 possesses a smaller semicircle than AC, affirming that the presence of RGO can increase the electrode conductivity. The cycling stability, another important measurement in the capacitor studies, was investigated by repeating the CV test in a potential range of -1 to 0 V at a scan rate of 70 mV s^{-1}. The NA-CRGO-1 shows a good capacitance retention ratio after 5000 cycles (Figure 6d), with only 7.7% decrease in the capacitance after 5000 cycles, which indicates an excellent cycling performance of the NA-CRGO-1 without any loss of the active material from the substrate.

4. CONCLUSION

In this work, we have developed a simple and low cost method for the fabrication of nitrogen doped activated composites containing a mixture of carbon derived from the agricultural waste material, and GO. The N-doped composites with spongy structure and high surface area were obtained by the single-step pyrolysis of the carbon/GO mixture using KOH and urea. The NA-CRGO-1 exhibited a high specific capacitance of 267 F g^{-1} at 5 mV s^{-1} in 6M KOH, which can be attributed to the coexistence of a double layer capacitance and pseudocapacitance phenomena. The NA-CRGO-1 showed a lower ESR compared to NA-CRGO-4 and good capacitance retention over 5000 cycles. The outstanding properties of the NA-CRGO-1 are attributed to a higher total N content (14.5 %) with appropriate species and distribution, the presence of GO, its high surface area. It was demonstrated that applying a

proper amount of activation and N-doping agents could produce a synthesized sample which can be used as capable electrode material for supercapacitors.

AUTHOR INFORMATION

Corresponding Authors

*E-mail: (S.F.S.Shirazi) f.shirazi@siswa.um.edu.my

Tel.: +60 142646276.

*E-mail: (S.Gharehkhani) s_gharahkhani_248@yahoo.com

Notes

The authors declare no competing financial interest.

ACKNOWLEDGEMENTS

This work was financially supported by the Ministry of High Education (MOHE) of Malaysia through grant number UM.C/ HIR/MOHE/ENG/45. Author 1 and Author 2 contributed equally to this work.

REFERENCES

1. A. Pandolfo and A. Hollenkamp, *Journal of power sources*, 2006, **157**, 11-27.
2. N. Devillers, S. Jemei, M.-C. Péra, D. Bienaimé and F. Gustin, *Journal of Power Sources*, 2014, **246**, 596-608.
3. Z. Endut, M. Hamdi and W. Basirun, *Thin Solid Films*, 2013, **528**, 213-216.
4. G. Wang, L. Zhang and J. Zhang, *Chemical Society Reviews*, 2012, **41**, 797-828.
5. G. A. Snook, P. Kao and A. S. Best, *Journal of Power Sources*, 2011, **196**, 1-12.
6. B. Xu, S. Yue, Z. Sui, X. Zhang, S. Hou, G. Cao and Y. Yang, *Energy & Environmental Science*, 2011, **4**, 2826-2830.
7. K. H. An, W. S. Kim, Y. S. Park, Y. C. Choi, S. M. Lee, D. C. Chung, D. J. Bae, S. C. Lim and Y. H. Lee, *Advanced Materials*, 2001, **13**, 497-500.
8. E. Frackowiak and F. Beguin, *Carbon*, 2002, **40**, 1775-1787.

9. W. H. Shin, H. M. Jeong, B. G. Kim, J. K. Kang and J. W. Choi, *Nano letters*, 2012, **12**, 2283-2288.
10. Z. Fan, J. Yan, T. Wei, L. Zhi, G. Ning, T. Li and F. Wei, *Advanced Functional Materials*, 2011, **21**, 2366-2375.
11. Z. Endut, M. Hamdi and W. Basirun, *Surface and Coatings Technology*, 2013, **215**, 75-78.
12. S. Yakout and A. Daifullah, *Desalination and Water Treatment*, 2014, **52**, 4485-4491.
13. P. R. Armstrong, Z. J. Morchesky, D. T. Hess, K. W. Adu, D. K. Essumang, J. K. Tufour, J. E. Koranteng-Addo, K. Opoku-Boadu and S. Y. Mensah, in *MRS Proceedings*, Cambridge Univ Press, 2014, pp. mrsf13-1644-dd1608-1601.
14. R.-L. Tseng and S.-K. Tseng, *Journal of Colloid and Interface Science*, 2005, **287**, 428-437.
15. V. Njoku, K. Foo, M. Asif and B. Hameed, *Chemical Engineering Journal*, 2014, **250**, 198-204.
16. T. Lee, Z. A. Zubir, F. M. Jamil, A. Matsumoto and F.-Y. Yeoh, *Journal of Analytical and Applied Pyrolysis*, 2014, **110**, 408-418.
17. S. Gharehkhani, E. Sadeghinezhad, S. N. Kazi, H. Yarmand, A. Badarudin, M. R. Safaei and M. N. M. Zubir, *Carbohydrate polymers*, 2015, **115**, 785-803.
18. G. K. Parshetti, S. K. Hoekman and R. Balasubramanian, *Bioresource technology*, 2013, **135**, 683-689.
19. L. Wei and G. Yushin, *Nano Energy*, 2012, **1**, 552-565.
20. X. F. Li, Q. Xu, Y. Fu and Q. X. Guo, *Environmental Progress & Sustainable Energy*, 2014, **33**, 519-526.
21. M. A. Yahya, Z. Al-Qodah and C. W. Z. Ngah, *Renewable and Sustainable Energy Reviews*, 2015, **46**, 218-235.
22. M. Sevilla and R. Mokaya, *Energy & Environmental Science*, 2014, **7**, 1250-1280.
23. L. Zhang, F. Zhang, X. Yang, G. Long, Y. Wu, T. Zhang, K. Leng, Y. Huang, Y. Ma and A. Yu, *Scientific reports*, 2013, **3**.
24. L. Jiang, J. Yan, Y. Zhou, L. Hao, R. Xue, L. Jiang and B. Yi, *Journal of Solid State Electrochemistry*, 2013, **17**, 2949-2958.
25. Z. Zhou and X.-F. Wu, *Journal of Power Sources*, 2013, **222**, 410-416.
26. M. D. Stoller, S. Park, Y. Zhu, J. An and R. S. Ruoff, *Nano letters*, 2008, **8**, 3498-3502.
27. S. Han, D. Wu, S. Li, F. Zhang and X. Feng, *Advanced Materials*, 2014, **26**, 849-864.
28. H. Kim, M. Y. Cho, M. H. Kim, K. Y. Park, H. Gwon, Y. Lee, K. C. Roh and K. Kang, *Advanced Energy Materials*, 2013, **3**, 1500-1506.
29. D. H. Seo, Z. J. Han, S. Kumar and K. K. Ostrikov, *Advanced Energy Materials*, 2013, **3**, 1250-1250.
30. F. Luan, G. Wang, Y. Ling, X. Lu, H. Wang, Y. Tong, X.-X. Liu and Y. Li, *Nanoscale*, 2013, **5**, 7984-7990.
31. B. Zhao, P. Liu, Y. Jiang, D. Pan, H. Tao, J. Song, T. Fang and W. Xu, *Journal of power sources*, 2012, **198**, 423-427.
32. M. Sookhakian, Y. Amin, R. Zakaria, W. Basirun, M. Mahmoudian, B. Nasiri-Tabrizi, S. Baradaran and M. Azarang, *Journal of Alloys and Compounds*, 2015, **632**, 201-207.
33. Y.-T. Weng, C.-B. Tsai, W.-H. Ho and N.-L. Wu, *Electrochemistry Communications*, 2013, **27**, 172-175.
34. M. Zhou, F. Pu, Z. Wang and S. Guan, *Carbon*, 2014, **68**, 185-194.
35. X. Hong, K. S. Hui, Z. Zeng, K. N. Hui, L. Zhang, M. Mo and M. Li, *Electrochimica Acta*, 2014, **130**, 464-469.
36. L. Zhao, L. Z. Fan, M. Q. Zhou, H. Guan, S. Qiao, M. Antonietti and M. M. Titirici, *Advanced Materials*, 2010, **22**, 5202-5206.
37. D. Hulicova-Jurcakova, M. Seredych, G. Q. Lu and T. J. Bandosz, *Advanced functional materials*, 2009, **19**, 438-447.
38. L.-F. Chen, Z.-H. Huang, H.-W. Liang, W.-T. Yao, Z.-Y. Yu and S.-H. Yu, *Energy & Environmental Science*, 2013, **6**, 3331-3338.

39. D. Hulicova, J. Yamashita, Y. Soneda, H. Hatori and M. Kodama, *Chemistry of materials*, 2005, **17**, 1241-1247.
40. E. Frackowiak, G. Lota, J. Machnikowski, C. Vix-Guterl and F. Béguin, *Electrochimica Acta*, 2006, **51**, 2209-2214.
41. J.-H. Kim, Y.-S. Lee, A. K. Sharma and C. G. Liu, *Electrochimica Acta*, 2006, **52**, 1727-1732.
42. Y. Tan, C. Xu, G. Chen, Z. Liu, M. Ma, Q. Xie, N. Zheng and S. Yao, *ACS applied materials & interfaces*, 2013, **5**, 2241-2248.
43. L. Zhao, N. Baccile, S. Gross, Y. Zhang, W. Wei, Y. Sun, M. Antonietti and M.-M. Titirici, *Carbon*, 2010, **48**, 3778-3787.
44. H.-B. Zhao, W.-D. Wang, Q.-F. Lü, T.-T. Lin, Q. Lin and H. Yang, *Bioresource technology*, 2014.
45. X. Y. Chen, C. Chen, Z. J. Zhang, D. H. Xie, X. Deng and J. W. Liu, *Journal of Power Sources*, 2013, **230**, 50-58.
46. J. Mi, X.-R. Wang, R.-J. Fan, W.-H. Qu and W.-C. Li, *Energy & Fuels*, 2012, **26**, 5321-5329.
47. D. Long, W. Li, L. Ling, J. Miyawaki, I. Mochida and S.-H. Yoon, *Langmuir*, 2010, **26**, 16096-16102.
48. Y. Li, Q. Du, T. Liu, X. Peng, J. Wang, J. Sun, Y. Wang, S. Wu, Z. Wang, Y. Xia and L. Xia, *Chemical Engineering Research and Design*, 2013, **91**, 361-368.
49. L. Khezami, A. Ould-Dris and R. Capart, *BioResources*, 2007, **2**, 193-209.
50. M. Lillo-Ródenas, D. Cazorla-Amorós and A. Linares-Solano, *Carbon*, 2003, **41**, 267-275.
51. T. Tay, S. Ucar and S. Karagöz, *Journal of Hazardous Materials*, 2009, **165**, 481-485.
52. L. Qie, W. Chen, H. Xu, X. Xiong, Y. Jiang, F. Zou, X. Hu, Y. Xin, Z. Zhang and Y. Huang, *Energy & Environmental Science*, 2013, **6**, 2497-2504.
53. Z. Lin, G. Waller, Y. Liu, M. Liu and C. P. Wong, *Advanced Energy Materials*, 2012, **2**, 884-888.
54. H. Sun, Y. Wang, S. Liu, L. Ge, L. Wang, Z. Zhu and S. Wang, *Chemical Communications*, 2013, **49**, 9914-9916.
55. Z. Fan, K. Wang, T. Wei, J. Yan, L. Song and B. Shao, *Carbon*, 2010, **48**, 1686-1689.
56. W. Xing, C. Liu, Z. Zhou, L. Zhang, J. Zhou, S. Zhuo, Z. Yan, H. Gao, G. Wang and S. Z. Qiao, *Energy & Environmental Science*, 2012, **5**, 7323-7327.
57. L. Sun, L. Wang, C. Tian, T. Tan, Y. Xie, K. Shi, M. Li and H. Fu, *RSC Advances*, 2012, **2**, 4498-4506.
58. K. Jurewicz, K. Babeł, A. Ziółkowski and H. Wachowska, *Journal of Physics and Chemistry of Solids*, 2004, **65**, 269-273.
59. S. Pilban-Jahromi, A. Pandikumar, B. T. Goh, Y. S. Lim, W. J. Basirun, H. N. Lim and N. M. Huang, *RSC Advances*, 2015.
60. G. Luo, L. Liu, J. Zhang, G. Li, B. Wang and J. Zhao, *ACS applied materials & interfaces*, 2013, **5**, 11184-11193.
61. R. Kötz and M. Carlen, *Electrochimica Acta*, 2000, **45**, 2483-2498.

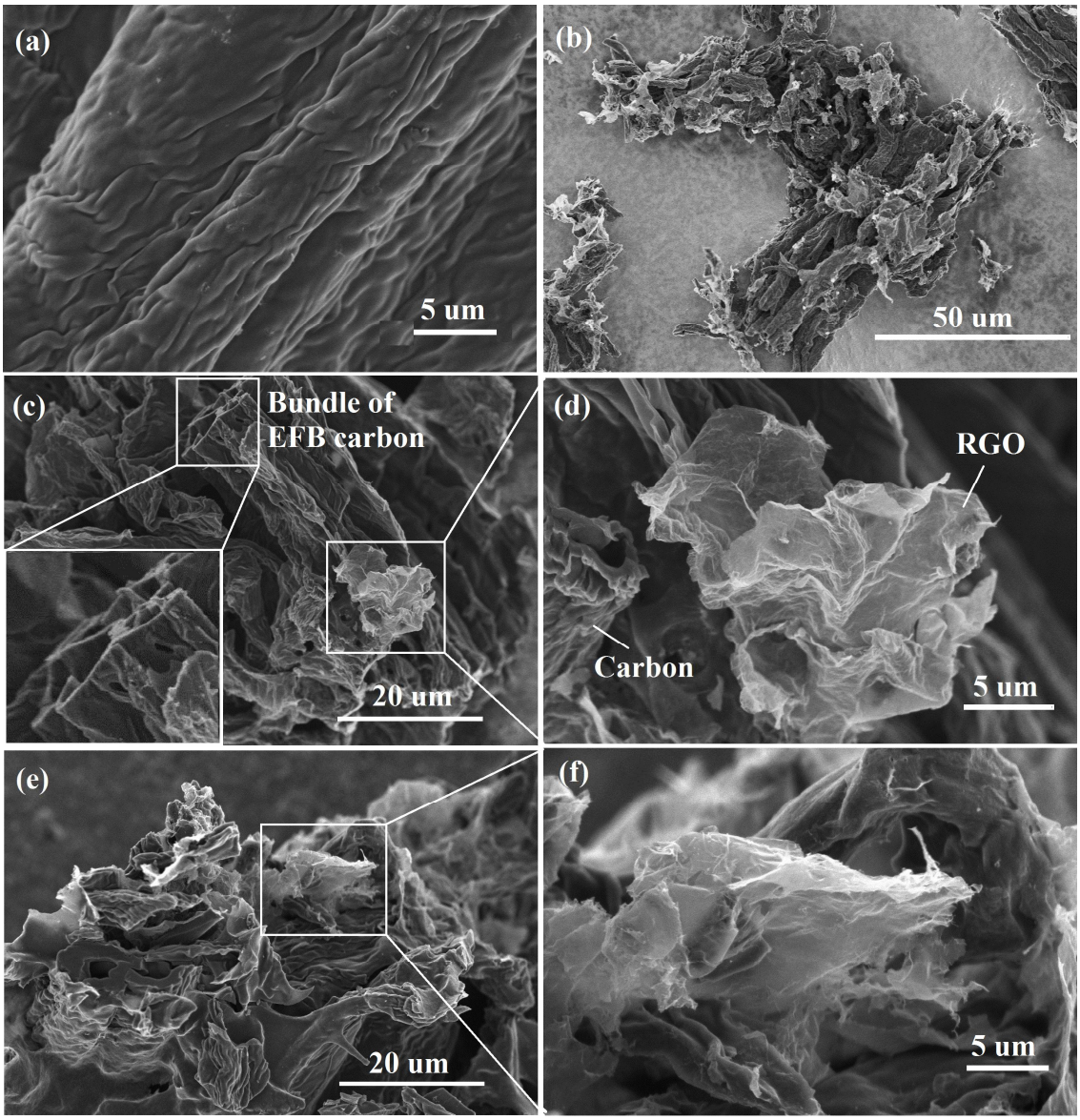

Figure 1. FESEM images of (a) Pure AC, (b-d) NA-CRGO-4 and (e and f) NA-CRGO-1.

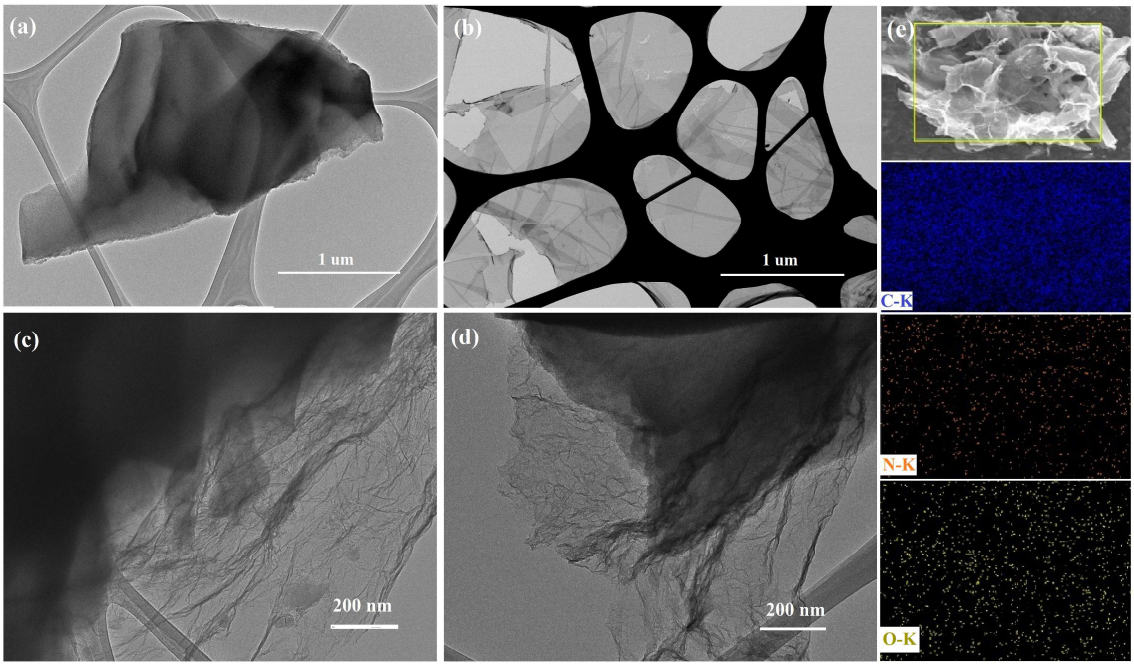

Figure 2. (a-d) TEM images of the AC, RGO, NA-CRGO-1 and NA-CRGO-4 respectively. (e) FESEM elemental mapping of NA-CRGO-1.

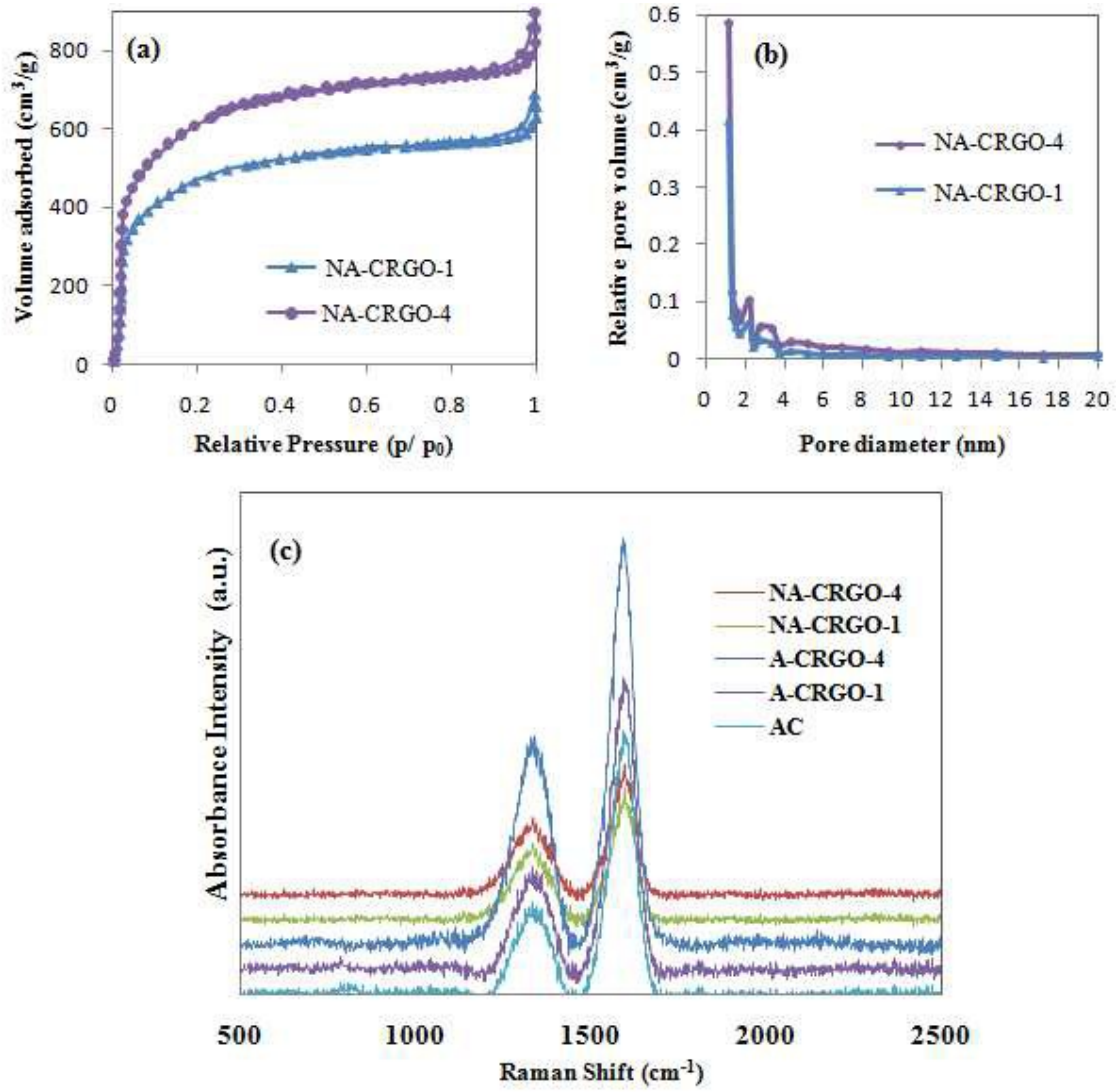

Figure 3. a) N_2 adsorption and desorption isotherms and b) Pore size distribution of N doped samples. c) The Raman spectra of samples

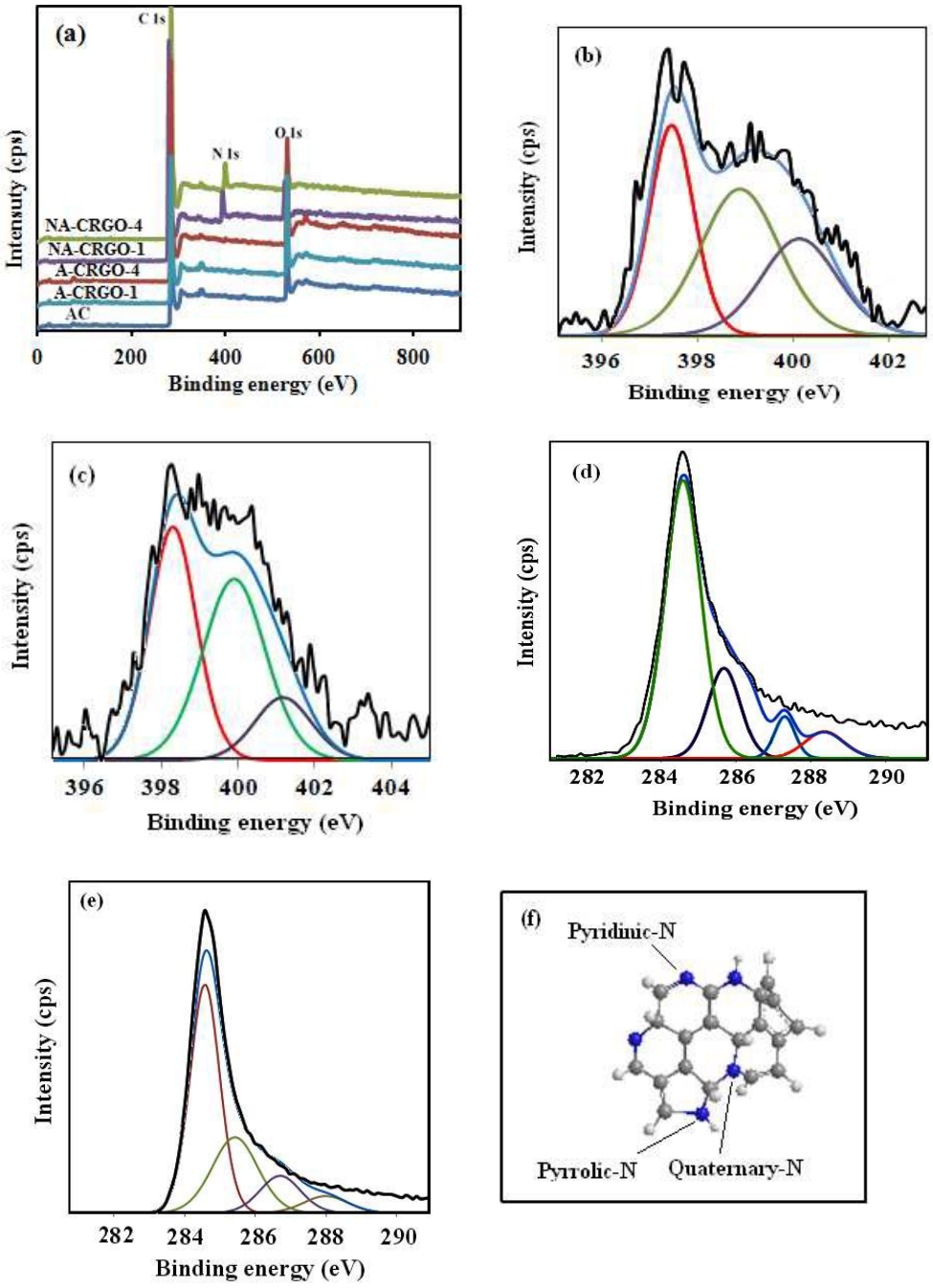

Figure 4. a) XPS survey spectra of all samples. (b and c) High-resolution N 1s spectra of NA-CRGO-1 and NA-CRGO-4. (d and e) High-resolution C 1s spectra of NA-CRGO-1 and NA-CRGO-4. f) A schematic structure of nitrogen surface functional groups on carbon.

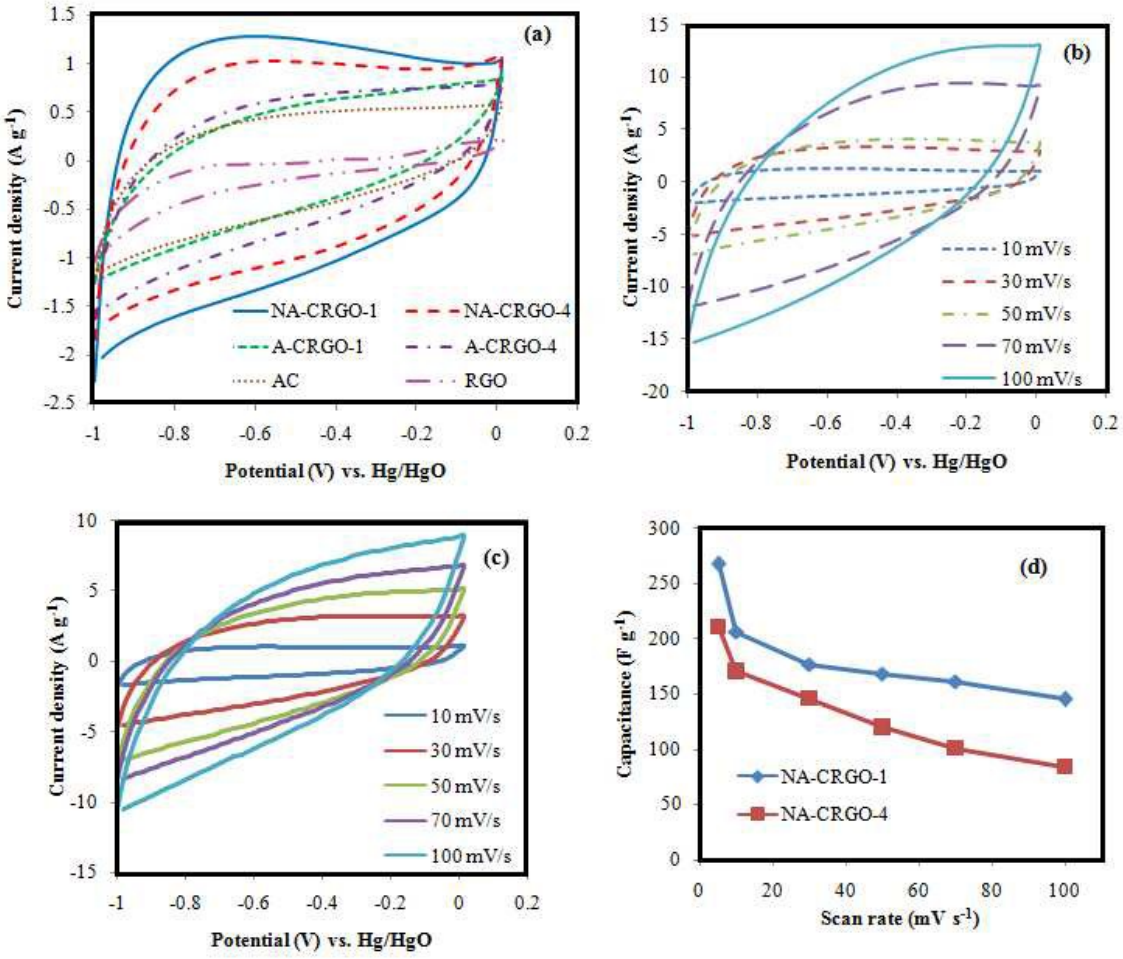

Figure 5. CV scans of the samples using a three-electrod cell in 6 M KOH; a) CV for doped and undoped samples at scan rate 10 mV s^{-1}. b) CV for NA-CRGO-1 at different scan rates. c) CV for NA-CRGO-4 at different scan rates. d) The relation between the specific capacitance and scan rate for NA-CRGO-1 and NA-CRGO-4.

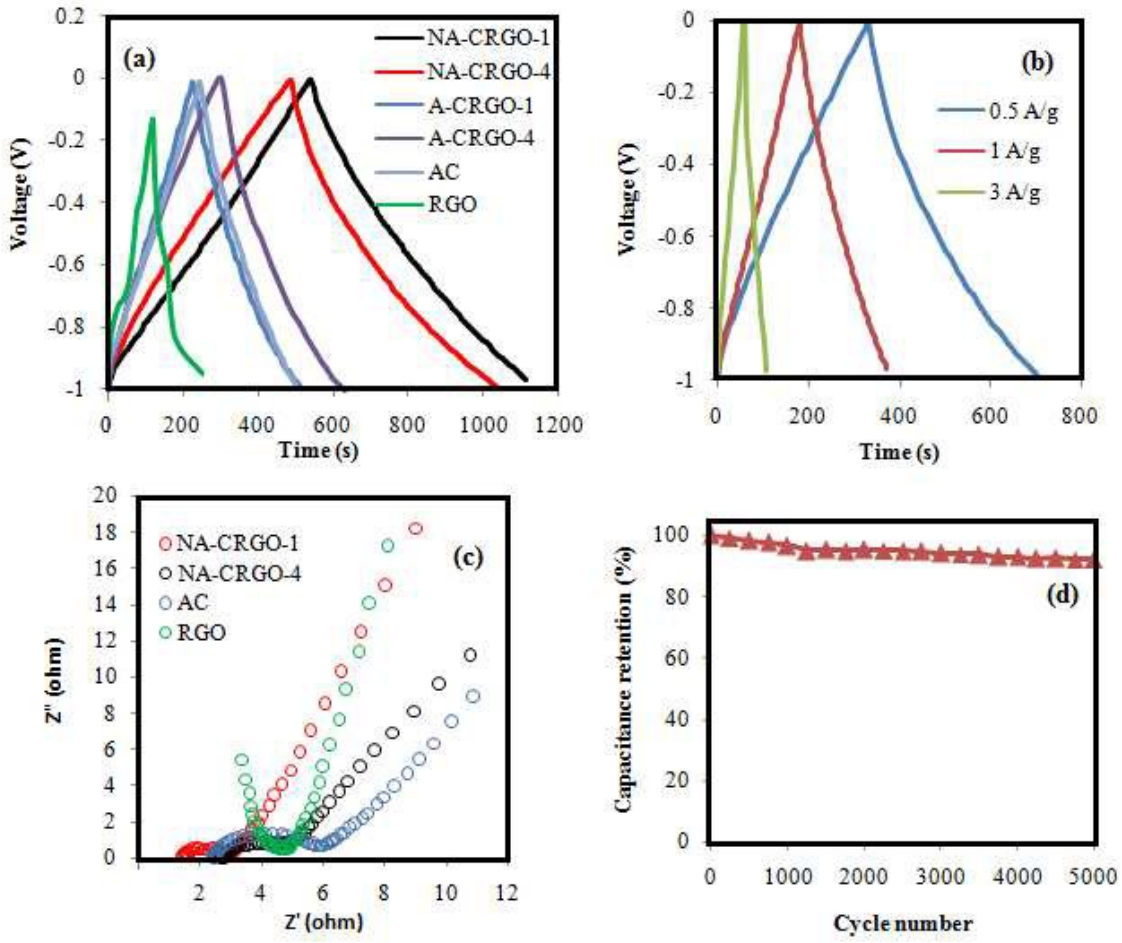

Figure 6. (a) Galvanostatic charge-discharge curves for all samples. (b) Galvanostatic charge-discharge curves for NA-CRGO-1 at different current densities. (c) Nyquist plots of NA-CRGO-1 and NA-CRGO-4, AC and RGO. (d) Capacitance retention ratio of NA-CRGO-1 after 5000 cycles at scan rate 70 mV s^{-1}.

Table 1. Pore structure of the N doped samples.

Sample	S_{BET} ($m^2 g^{-1}$)	Total pore volume($cm^3 g^{-1}$)	Micropore volume ($cm^3 g^{-1}$)	Mesopore volume ($cm^3 g^{-1}$)
NA-CRGO-1	1712.4	0.93	0.69	0.24
NA-CRGO-4	2261.2	1.31	0.84	0.46

Table 2. The chemical composition of samples evaluated by (XPS)

Sample	C (atom %)	O (atom %)	N (atom %)	N1	N2	N3	N/C
AC	59.65	40.35	-	-	-	-	-
A-CRGO-1	79.02	20.98	-	-	-	-	-
A-CRGO-4	65.50	34.50	-	-	-	-	-
NA-CRGO-1	68.95	16.54	14.51	5.29	5.85	3.36	0.21
NA-CRGO-4	74.09	14.38	11.53	4.85	5.08	1.60	0.15

Graphical Abstract

A nitrogen doped and activated material with spongy-like structure containing a low cost carbon derived from the waste agricultural material and graphene oxide is synthesized via facile thermal treatment for supercapacitor applications.